2021

A Local Similarity Function for Katabatic Flows Derived From Field Observations Over Steep- and Shallow-Angled Slopes

Chaoxun Hang

Holly J. Oldroyd

Marco G. Giometto

Eric R. Pardyjak

Marc B. Parlange
University of Rhode Island, marc.parlange@uri.edu

A Local Similarity Function for Katabatic Flows Derived From Field Observations Over Steep- and Shallow-Angled Slopes

Chaoxun Hang[1] ⓘ, Holly J. Oldroyd[2] ⓘ, Marco G. Giometto[3], Eric R. Pardyjak[4] ⓘ, and Marc B. Parlange[5] ⓘ

[1]School of Oceanography, Shanghai Jiao Tong University, Shanghai, China, [2]Department of Civil and Environmental Engineering, University of California Davis, Davis, CA, USA, [3]Department of Civil Engineering and Engineering Mechanics, Columbia University, New York City, NY, USA, [4]Department of Mechanical Engineering, University of Utah, Salt Lake City, UT, USA, [5]Department of Civil and Environmental Engineering, University of Rhode Island, Kingston, RI, USA

Abstract Katabatic flows are notoriously difficult to model for a variety of reasons. Notably, the assumptions underpinning Monin-Obukhov similarity theory (MOST) are inherently violated by the sloping terrain, causing the traditional flux-gradient relations used in numerical weather prediction models to break down. Focusing on turbulent momentum transport, we show significant flux divergence, further violating MOST assumptions, and that the traditional parameterizations fail even with local scaling for katabatic flow. In response, we propose a modified local-MOST stability-correction function, informed by near-surface turbulence observations collected over two mountainous slopes with inclination angles (α) of $\alpha \approx 7.8°$ and $\alpha \approx 35.5°$. The proposed relation includes α directly, making data from both slopes collapse with unprecedented agreement. RMSE between measured fluxes and estimates from the proposed and Businger et al. (1971, https://doi.org/10.1175/1520-0469(1971)028<0181:FPRITA>2.0.CO;2) relations show significant improvement. Results can be used to inform future development of wall-model and turbulence closures in the katabatic flow layer.

Plain Language Summary Katabatic flows form by colder (higher density) air, caused by surface cooling, descending along a slope under the force of gravity. They are notoriously difficult to represent in numerical weather prediction models for a variety of reasons. Most notably, these numerical models use an equation for turbulent momentum transport, which translates how surface conditions impact the atmosphere (and vice versa), which fails for katabatic flows because it was developed using measurements from sites over horizontal, homogeneous land surfaces. In this work, we focus on turbulent momentum transport and show stark differences between observations from katabatic flows and the traditional predictions. To address these critical problems, we propose a modified equation, informed by near-surface turbulence observations collected over two mountainous slopes with different inclination angles (α), $\alpha \approx 7.8°$ and $\alpha \approx 35.5°$. The proposed equation includes α directly and shows unprecedented agreement with katabatic flow data. Results can be used to inform future development of numerical simulations of katabatic flows to better relate the sloping terrain and their influences on the near-surface atmosphere.

1. Introduction

Katabatic flow initiates over sloping terrain under a stably stratified atmosphere due to the surface radiative cooling. As the surface temperature cools, air near the ground becomes negatively buoyant with respect to air farther away from the slope at the same elevation and starts descending down the slope. The ambient environment and surface friction impose a drag force near the surface, thus causing a jet-like wind profile. Such flows are ubiquitous in nature over sloping mountainous terrains (Whiteman, 2000).

Katabatic flows have a wide range of applications across different spatial and temporal scales. Over stably stratified mountainous terrain, such flows strongly affect the turbulent transport of momentum and scalars (Denby & Smeets, 2000; Grisogono & Oerlemans, 2001b; Mahrt, 1998; Monti et al., 2002; Stiperski et al., 2019), fog evolution (Hang et al., 2016; Román-Cascón et al., 2015), atmospheric dispersion and air quality (Lee et al., 2003; Pardyjak et al., 2009), wind energy (Clifton et al., 2014), and ecosystem environments (Pypker et al., 2007). Over glaciers and ice sheets, katabatic winds also play an important role on turbulent transport of surface mass and energy balances, which directly affect the weather and climate in polar regions (Forrer & Rotach, 1997; Oerlemans et al., 1999) as well as impacting water resources through mountain glacier recession (van den Broeke, 1997;

Methodology: Chaoxun Hang, Holly J. Oldroyd, Eric R. Pardyjak, Marc B. Parlange
Supervision: Marc B. Parlange
Writing – original draft: Chaoxun Hang
Writing – review & editing: Holly J. Oldroyd, Marco G. Giometto, Eric R. Pardyjak, Marc B. Parlange

Smeets et al., 1998). Strong, persistent katabatic winds coming off of Antarctica also maintain open water polynyas by pushing sea ice away from the coast and impacting ice formation, ocean temperatures and the marine ecosystem (Bromwich & Kurtz, 1984; Ebner et al., 2014; Paterson et al., 2015; Wenta & Cassano, 2020). A profound understanding of katabatic flows and the associated turbulent transport are critical parts of numerical modeling and predicting these flows for such applied studies involving sloping terrain.

Based on Prandtl (1942)'s pioneering work on the analytical theory for slope flows, the mean profiles in real katabatic winds have been qualitatively well understood for some time (Papadopoulos et al., 1997). There have been numerous field campaigns focused on measuring mean quantities of katabatic flows, but far fewer have been designed to measure turbulence quantities at multiple heights above ground level (cf. Horst & Doran, 1986; Smeets et al., 1998; Monti et al., 2002). Yet, the turbulent transport associated with slope flows is poorly understood due to the complex dynamics (e.g., flow processes on different time and space scales, energy balance complexities, surface heterogeneity, and roughness, etc.) that are associated with stably stratified boundary layers (Grisogono & Oerlemans 2001a, 2001b; Grisogono & Axelsen, 2012; Shapiro & Fedorovich, 2014) as well as the challenges associated with obtaining representative field observations over sloping terrain. Recently, higher-resolution datasets that contain turbulence measurements above and below the wind maxima of katabatic jets have become available. Examples include: a slope in Val Ferret, Switzerland (Nadeau et al., 2013; Oldroyd et al., 2014; Oldroyd, Pardyjak, Higgins, et al., 2016), a slope from the MATERHORN field campaign (Grachev et al., 2016; Hang et al., 2020; Jensen et al., 2017), within and near the Arizona Meteor Crater (Lehner et al., 2016; Stiperski et al., 2019), and in the valley of Grenoble in the French Alps (Charrondière et al., 2020). Analyses of these datasets have begun to yield an improved understanding of the real modeling limitations and challenges associated with slope flows such as turbulence flux divergence, the importance of along-slope buoyancy fluxes on stability, and the turbulence structure below and above the jet peak.

One of the most critical needs related to slope-flow applications is to better model the katabatic flows very close to the surface, where the sharpest gradients of wind and temperature exist. Specifically, more suitable turbulence parameterizations for katabatic flows near the slope surfaces are needed. Similarity theory aims to develop a universal description of relations between different flow variables and is useful in boundary-layer meteorology when complicated dynamics elude deterministic descriptions (Stull, 1988). Monin-Obukhov similarity theory (MOST) (Monin & Obukhov, 1954) has been widely used in numerical weather prediction as well as hydrology, climate and wind-energy models as a scaling framework for developing empirical parameterizations for near-surface turbulence fluxes (Businger et al., 1971; Chenge & Brutsaert, 2005; Dyer, 1974; Högström, 1988; Stull, 1988). However, MOST, which was empirically developed for horizontal and homogeneous terrain, has been shown to be inadequate for stable boundary layers (Mahrt, 2014, and references therein) and particularly, for katabatic flows due to significant flux-divergence contributions in the slope-normal (and vertical) direction (Giometto et al., 2017; Grachev et al., 2016; Grisogono & Rajak, 2009; Grisogono et al., 2007; Nadeau et al., 2013; Oldroyd et al., 2014). To address shortcomings associated flux divergence, Nieuwstadt (1984) reformulated MOST in terms of local scaling instead of characteristic constant-flux surface-layer values. Several recent studies of the near-surface turbulence in katabatic flows over mountainous terrain provide adequate resolution to explore this flux divergence and its implications for local flux-gradient similarity scaling (Charrondière et al., 2020; Grachev et al., 2016; Nadeau et al., 2013; Oldroyd et al., 2014; Oldroyd, Pardyjak, Higgins, et al., 2016; Stiperski et al., 2019).

Notwithstanding the limitations of MOST similarity functions, numerical simulations of katabatic flows are routinely carried out using the constants derived from flat, horizontal, and homogeneous terrains (see e.g., Axelsen & van Dop, 2009a, 2009b). It is hence desirable to have a more representative stability correction function for thermally driven flows over sloping surfaces.

The objectives of this work are:

1. To identify katabatic flow regimes from datasets for two slopes with different slope angles (i.e., 7.8° and 35.5°).
2. To analyze the turbulence flux divergence and structure below and above the jet peak (wind maximum) ffor katabatic winds.
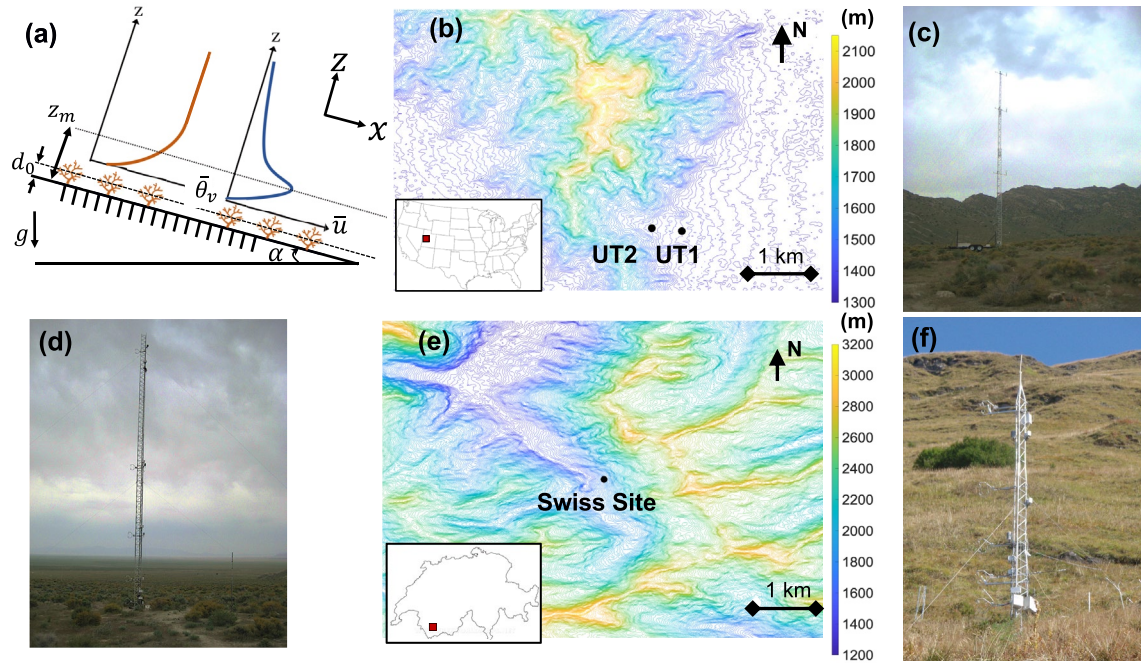
Figure 1. (a) Slope-following coordinate system with the x-axis directed downslope with angle, α, and the z-axis directed perpendicular to the slope. The sketches of $\bar{u}$ (streamwise velocity) and $\bar{\theta}_v$ (virtual potential temperature) show the theoretical profiles during katabatic events. z_m is the height of wind maxim, or jet peak, d_0 is the mean displacement height and g represents the gravitational vector; (b) location and elevation contours of Granite Mountain; (c) and (d) turbulence flux towers at UT1 and UT2 sites, respectively; (e) location and elevation contours in the Val Ferret Valley; (f) turbulence flux tower at the Swiss site.

3. To explore whether katabatic flows are amenable to local similarity scaling via near-surface turbulence observations collected from the two mountainous slopes despite an order of magnitude difference in slope angles (α).

2. Background

To approach this problem, a slope-following Cartesian coordinate system is used with the x-axis pointing downslope, and z-axis perpendicular to the slope (Figure 1a).

A local-similarity function can be defined as:

$$\phi_m\left(\zeta\right) = \frac{k\left(z - d_0\right)}{u_*}\frac{d\bar{u}}{dz} \tag{1}$$

where ϕ_m is the dimensionless wind shear, k is von Kármán constant (0.4 in this study), d_0 is the mean displacement height (0.27 m at UT1, 0.39 m at UT2, and 0.23 m at Swiss site), $u_* = \left[\left(\overline{u'w'}\right)^2 + \left(\overline{v'w'}\right)^2\right]^{1/4}$ is the local friction velocity, $\bar{u}$ is the mean wind speed in streamwise direction, $\bar{v}$ and $\bar{w}$ are the spanwise and surface-normal velocities, respectively, the local atmospheric stability parameter ζ is defined as:

$$\zeta \equiv \frac{z - d_0}{\Lambda} \tag{2}$$

where Λ is the local Obukhov length (Nieuwstadt, 1984; Obukhov, 1971) written as:

$$\Lambda = -\frac{u_*^3\,\theta_{v0}}{\kappa\,g\,\overline{w'\theta_v'}} \tag{3}$$

where, θ_{v0} is a characteristic virtual potential temperature, $\overline{w'\theta_v'}$ is the kinematic heat flux, and g is the gravitational acceleration. Overbars represent mean quantities; primes indicate turbulent perturbations from the mean. In this work, gradients of wind speed were calculated by curve fitting the observational data at all levels and computing the derivative with respect to z. The interpolation scheme is $\overline{u}(z) = a \ln(z) + bz^2 + cz + d$ (Forrer & Rotach, 1997), which is the best fit to the data profiles.

The most used form of flux-gradient relation under stable conditions is:

$$\phi_m(\zeta) = 1 + \beta_m \zeta, \tag{4}$$

where the empirical constant β_m is typically determined by field observations. Over horizontal, homogenous, flat terrain, Businger et al. (1971) found $\beta_m = 4.7$ with $\kappa = 0.35$. Later on, Dyer (1974) modified them as $\beta_m = 5.0$ with $\kappa = 0.41$. Högström (1988) re-evaluated early work and summarized that $\beta_m = 4.8$, when $\zeta \leq 0.5$; $\beta_m = 6$, when $\zeta > 0.5$. While the empirical constants above can work well for the evaluation of surface fluxes in stably stratified conditions for shear-driven flow over horizontal and homogeneous terrain, their use in katabatic-flow regimes is not justified on a theoretical ground, thus introducing a degree of uncertainty in model results that needs to be addressed (Grachev et al., 2016; Heinemann, 2004; Smeets et al., 1998; van der Avoird & Duynkerke, 1999).

3. Methodology

Data were collected over a shallow and a substantially steeper slope. The first data set described is from the field campaigns of the Mountain Terrain Atmospheric Modeling and Observations (MATERHORN) program (more details can be found in Fernando et al., 2015). The second corresponds to measurements from Val Ferret, a narrow alpine valley in Switzerland (Figure 1e).

3.1. The MATERHORN Site

At the primary observation sites, two turbulence flux towers (UT1, UT2, also known as ES4 and ES5 from MATERHORN program) were deployed along the slope of Granite Mountain (Figure 1b). UT1 and UT2 sit in the canyon-like upper part of the slope with slope angles of 7.5° and 8°, respectively. The slope angle was determined via the Google Earth application. The surface is covered by sparse, desert-steppe vegetation with an average height of 1 m. Each tower was instrumented with a minimum of five levels of 3-D ultrasonic anemometers to measure turbulence (Figures 1c and 1d). Mean and turbulence variables were averaged over 5-min intervals to avoid the interference from sub-meso and wave motions while still capturing the rapid katabatic flow dynamics. The selection of the time-averaging interval was verified using a multiresolution decomposition (MRD) analysis of kinematic heat and momentum fluxes (Vickers & Mahrt, 2003) and ogive test (Aubinet et al., 2012). A two-sector planar fit was used with the sectorwise planar-fit coefficients computed from 30-min averaged wind data (Wilczak et al., 2001). Note that only 2-m observations were used for the analysis the of similarity functions below the jet peak, since the lowest level (i.e., 0.5 m) is within the canopy layer height ($\sim$1 m). More details can be found in Grachev et al. (2016) and Jensen et al. (2017).

3.2. The Swiss Site

The Swiss site is located in a characteristic Alpine valley, where a steep slope ($\alpha \approx 35.5°$) is covered by Alpine grasses and flowers of the order of 0.3 m (Figure 1e). The turbulence flux tower was equipped with five levels of 3-D ultrasonic anemometers to measure the turbulence. In addition, the anemometers were mounted in a slope-normal-slope-parallel coordinate system. Data were averaged over 10-min blocks, which was selected based on MRD (Vickers & Mahrt, 2003) and Fourier co-spectral ogive analyses (Babić et al., 2012). Optimized sector-wise planar fit was applied during the data processing. More details are presented in Oldroyd, Pardyjak, Huwald, et al. (2016).

For both MATERHORN and Swiss sites, katabatic events formed during clear sky and weak synoptic conditions, and were identified with the following criteria:

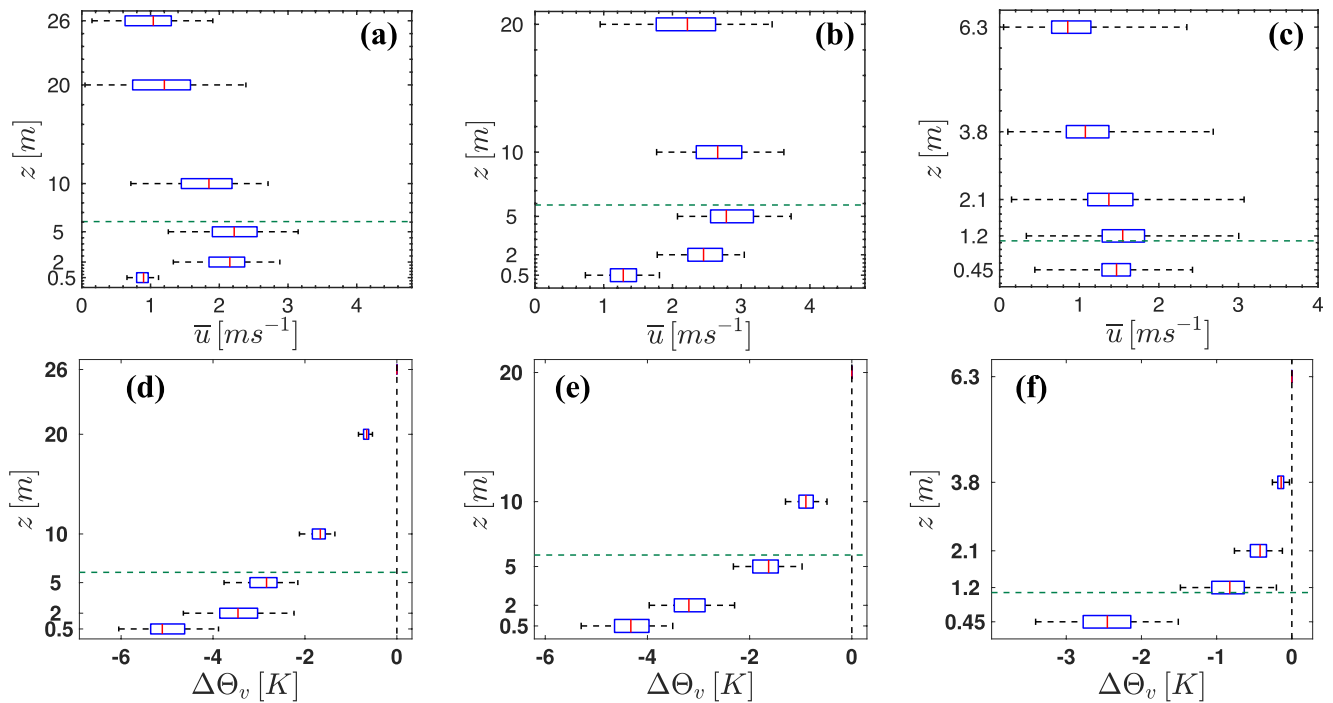1. The profile of streamwise wind speed has a jet-like shape.

Figure 2. Box plots of mean streamwise wind speed at (a) UT1, (b) UT2, and (c) Swiss site and virtual potential temperature deficit at (d) UT1, (e) UT2, and (f) Swiss sites during katabatic flow periods. Green dashed lines represent the median estimated heights of jet peaks, which are 6.15, 6.01, and 1.15 m for UT1, UT2, and Swiss sites, respectively.

    2. The mean wind direction is down the slope.

    3. The virtual potential temperature monotonically increases with distance from the surface.

From these criteria with the selected averaging times, the statistics are based on, 430 samples for UT1, 215 samples for UT2, and 521 samples for Swiss site.

4. Results and Discussion

4.1. Katabatic Mean-Flow Characteristics

To characterize the dynamics of katabatic flows at the study sites, we show box plots of stream-wise wind speed at different measurement levels at all three sites. From Figures 2a–2c, we can see well-developed katabatic flows with jet-like wind profiles at all sites. The jet peak height is estimated as the height where the linearly interpolated slope-normal momentum fluxes, $\overline{u'w'}$, crosses zero (Grachev et al., 2016). The medians of the jet-peak heights are 6.15, 6.01, and 1.15 m for UT1, UT2, and Swiss sites, respectively (represented by green dashed lines in Figure 2), and they are highly consistent with narrow interquartile ranges.

There are similarities between the two slope sites in terms of flow structure for katabatic winds despite the differences between wind maxima height and katabatic layer depth, which are related to the differing slope angles over slopes with lengths of the same magnitudes. Both flows have well-developed low-level jets with maximum turbulence quantities, such as TKE and slope-normal heat flux, near the ground (not shown here). Strong (negative) vertical momentum fluxes can be observed below the jet peak that monotonically decrease to zero as the jet peak height is approached (Figure 3). In addition, wind maxima are within the temperature-inversion layer, where the strongest static stability favors the formation of katabatic winds (Figures 2d–2f).

Virtual potential temperature deficit $\Delta\Theta_v$ is estimated by the difference between local Θ_v and atmospheric ambient Θ_v, which is assumed as the temperature measurement at the top level in this study. Figures 2d–2f show box plots of $\Delta\Theta_v$ at all measurement levels at different sites during katabatic events. Below the estimated jet peak heights (indicated by green dashed lines in the figure), negative $\Delta\Theta_v$ indicates a statically stable stratified
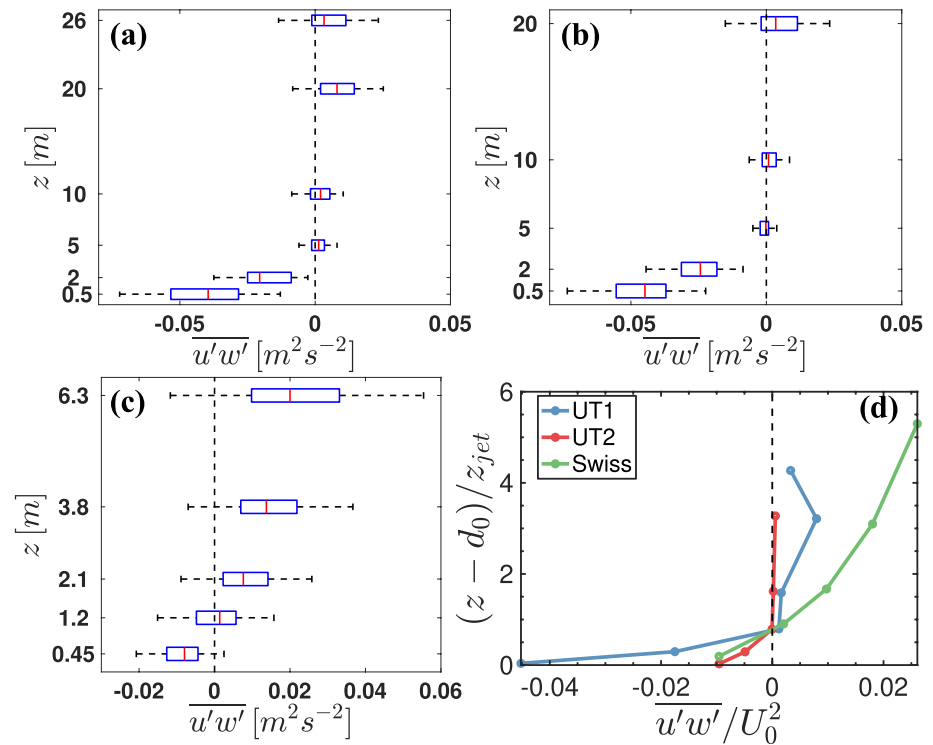
Figure 3. Box plots of slope-normal momentum fluxes at (a) UT1, (b) UT2, and (c) Swiss site during katabatic periods, (d) medians of normalized momentum fluxes at UT1, UT2, and Swiss sites versus normalized slope-normal height during katabatic flows. U_0 is the streamwise wind speed at the top measurement level, as the ambient wind speed of atmosphere.

near-surface layer at all sites with strong temperature gradients over a very shallow layer. Above the jet peak, are much weaker gradients especially at the near upper two levels.

4.2. Variations of Turbulence Momentum Fluxes

The applicability of similarity functions has not been thoroughly assessed through observed turbulence fluxes for katabatic winds over multiple sites with drastically different slope angles. In this work, slope-normal momentum fluxes at multiple levels are evaluated, which include turbulence measurements below and above the jet peak of katabatic flows.

As the slope-normal wind gradients, $d\bar{u}/dz$, change sign from below to above the jet peak, the momentum fluxes are expected to cross zero from negative to positive, which is illustrated in Figure 3 at all field sites. To assess the turbulent transport across the katabatic layer, we separate the flow layer into two regions, namely below the jet peak, which contains the layer above the vegetation and below the wind maxima height, and above the jet peak to the top of the katabatic flow layer. Below the jet peak, all three sites display a similar trend of $\overline{u'w'}$, with magnitudes decreasing as the height increases. In this region, the vertical momentum flux is dominated by the surface stress generated from the surface roughness (i.e., 1-m sparse, desert steppe at UT1 and UT2, 0.3 m Alpine grasses and flowers at Swiss). Above the jet peak, $\overline{u'w'}$ is relatively constant and near zero at UT sites (Figures 3a, 3b, and 3d) whereas, at the Swiss site, $\overline{u'w'}$ monotonically increases as the height increases (Figures 3c and 3d). Previous work of Oldroyd et al. (2014) showed that the vertical momentum flux departs from zero as the larger-scale pressure perturbation penetrates down to the surface level. Slope-normal profiles of $\overline{u'w'}$ at the UT sites (Figure 3d) may imply that the entrainment from the ambient atmosphere toward the katabatic flow is too weak to create significant $\overline{u'w'}$ divergence above the jet peak.
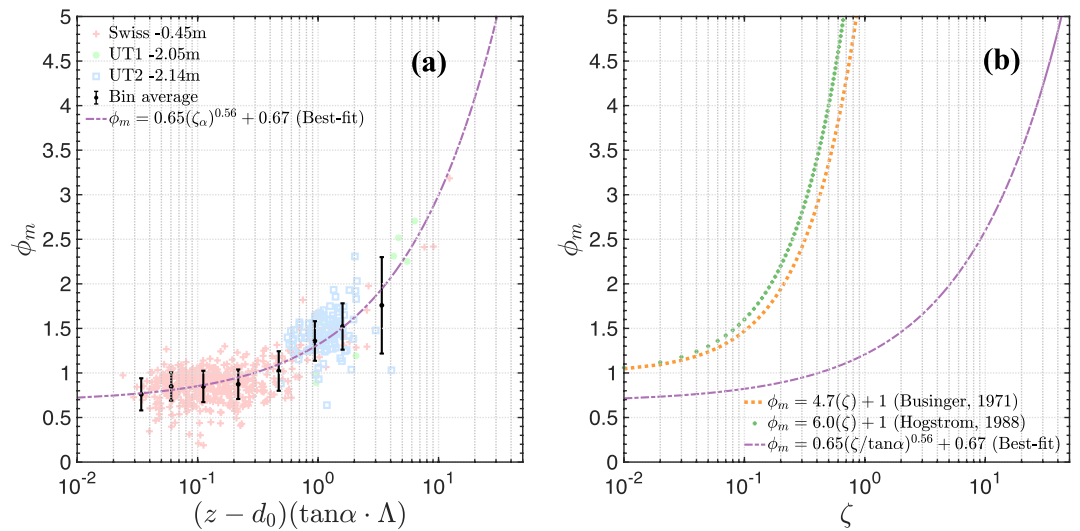
Figure 4. (a) Normalized wind shear ϕ_m versus $(z - d_0)/(\tan(\alpha) \cdot \Lambda)$. Data from UT sites are 2 m above the ground level, and data from Swiss site is 0.45 m above ground level, both are below the jet peak heights and above the canopy. The dashed purple line is a best fit of the data. Error-bars show the standard deviations of the observational data. (b) Comparison of flux-gradient relations between best fit from this study and the classical ones.

4.3. Flux-Gradient Relations

Understanding the behavior of the flux-gradient relations is crucial for the parametrization of turbulent transport physics in many types of flows. We have seen in previous research (e.g., Nadeau et al., 2013) that classic flux-gradient relations are not applicable over mountain slopes above and near the katabatic jet peak. Very few studies explored the katabatic flow structure specifically below the jet peak (cf. Charrondière et al., 2020; Grachev et al., 2016; Oldroyd et al., 2014; Stiperski et al., 2019). To generalize the similarity functions over slopes, we include slope angle as a variable in the original local-MOST scaling framework, for which any trigonometric function of the slope angle becomes dimensionless. For a slope-aligned coordinate system (see Figure 1a), the ratio between slope-normal and along-slope heat fluxes, along with the cotangent of the slope angle, determines whether buoyancy produces or suppresses turbulence kinetic energy over the slope (Horst & Doran, 1986). One of the key findings from Oldroyd, Pardyjak, Higgins, et al. (2016) is that the ratio between slope-normal and along-slope heat fluxes is not a simple linear function of slope angle, and that buoyant TKE production can occur even over relatively shallow slopes. When this flux ratio is greater than $1/\tan\alpha$ (for the coordinate system in Figure 1a) TKE is buoyantly produced, making $\tan\alpha$ a logical approach to nondimensionalize the slope angle for similarity analyses. Hence, a modified atmospheric stability parameter is defined here as

$$\zeta_\alpha = \frac{(z - d_0)}{(\tan\alpha \cdot \Lambda)}. \tag{5}$$

Note that the intention of utilizing the tangent function is not to universalize the flux-gradient relation and/or atmospheric stability parameter for both horizontal and sloping surfaces, but rather specifically for katabatic flows, which exhibit a jet-shaped profile. Consequently, when the slope angle α approaches zero, ζ_α does not converge to classic ζ over horizontal surfaces. Also note that other trigonometric functions were considered, but they did not readily lead to a parameterization that collapsed for both slope angles.

Figure 4a shows normalized wind shear ϕ_m versus the modified atmospheric stability parameter ζ_α under the jet peak. Again, note that only 2-m measurements at UT sites are used here. The lowest level (i.e., 0.5 m) is eliminated from this analysis due to the fact that the observation is within the canopy height (~1 m). Data from the two-slope sites collapse surprisingly well within the modified stability range of 0.01–10, despite the significant differences in slope angles, depths of the slope-flow layers, climate regions, and vegetation cover. Figure 4b indicates a significant difference between the newly modified profile and the classical ones (e.g., Businger et al., 1971;

Högström, 1988), which were developed over horizontal homogeneous and horizontal surfaces. RMSE between the normalized momentum fluxes from proposed relation and data is 0.20, which is significantly lower than 4.65 that is calculated between the classic Businger et al. (1971) relation and data. The modified local flux-gradient relation can be written as:

$$\phi_m = 0.65\zeta_\alpha{}^{0.56} + 0.67 \qquad (6)$$

which holds below the jet peak height even for this large range of slope angles. Note that above the katabatic jet peak, the data do not collapse across sites. This is likely caused by turbulence decoupling from the surface, as the momentum fluxes approach zero at the jet peak, and hence, being governed by different physical mechanisms. However, these above-peak data also indicate enhanced mixing (lower ϕ_m, arguments below) compared to the horizontal terrain relations (not shown). The new flux-gradient relation for katabatic flow is not constrained by using the classic logarithmic velocity profiles within the surface layer under neutral stability conditions. In other words, without confirming the validation of the logarithmic velocity profile over slopes, the intercept of the flux-gradient relation does not necessarily equal unity.

If we rearrange the scaling of the normalized momentum flux and replace the friction velocity by the vertical momentum flux (i.e., $-\overline{u'w'} = u_* \cdot u_*$), we will have:

$$\overline{u'w'} = \left(\frac{k \cdot z \cdot u_*}{\phi_m} \right) \cdot \frac{d\overline{u}}{dz} \qquad (7)$$

By analogy with gradient-transport theory (also known as K-theory), $\left(k \cdot z \cdot u_*/\phi_m \right)$ can be considered a turbulent transfer coefficient with the atmospheric stability correction function, ϕ_m (e.g., Arya, 2001), such that as ϕ_m increases, turbulent mixing decreases. From Figure 4b, we can see that at any given stability ζ, ϕ_m over slopes is less than what is predicted by the relations for horizontal surfaces. This indicates that turbulent mixing is generally stronger for slope flows than for flows over horizontal surfaces at the same ζ. Greater turbulent mixing below the jet peak of katabatic flows is a result of enhanced shear stress generated by the jet-shaped velocity profile during stable conditions. As the atmosphere becomes more stable (i.e., ζ increases), turbulent mixing strength over both horizontal and inclined surfaces (at least below the nose of the jet) gets weaker since the stratified atmosphere suppresses turbulence. However, ϕ_m increases more slowly for katabatic flows than for flows over horizontal surfaces. In other words, as the atmosphere becomes more stable and turbulent mixing is inhibited, the rate of change of ϕ_m in katabatic flows is less than that for horizontal-surface flows. While the negative buoyancy force increases the atmospheric stability, it is also the driving force in the momentum equation for katabatic flows. This enhancement of turbulent mixing through shear partially compensates the suppression of turbulence by the stratified atmosphere, which leads to a lower rate of decreasing mixing for katabatic winds. Results from Łobocki (2014), who used a second-order turbulence closure model for slope flows to solve for ϕ_m for different slope angles, also show an enhanced mixing in katabatic flow compared to horizontal terrain.

4.4. Assessment of Self-Correlation

Any attempt to evaluate similarity functions in the MOST framework should assess self-correlation according to Mahrt (1998). The correlation induced by u_* on both sides of flux-gradient relations may result in a misleading confidence in the applicability of MOST-similarity functions. To evaluate this, we followed the work proposed by Klipp and Mahrt (2004) by using random sampling with replacement to assess potential impacts of self-correlation. At a given level, z, datasets of ϕ_m and ζ_α are generated randomly from the original observations of $\overline{w'\theta'}$, u_*, and $\partial\overline{u}/\partial z$. We compute the linear-correlation coefficient between ϕ_m and ζ_α by using the random data. This process is repeated 1000 times to eliminate any physical connections between the variables.

For the UT sites at 2-m level and the Swiss site at 0.45-m level, the linear-correlation coefficient for the original data, R_{data}, is 0.45, and the averaged correlation coefficient for 1000 random datasets, $\langle R_{\text{random}} \rangle$, is 0.25 with a standard deviation of 0.09. The reduced correlation coefficient for the randomized data set indicates that self-correlation has little impact on the similarity results.

5. Conclusions

In this work, we explored the flux-gradient relations of streamwise wind speed during katabatic events at three field sites: stations UT1 and UT2 from the MATERHORN program at Granite Mountain have an average slope angle of 7.8°, and the Val Ferret site in Switzerland that has a local slope angle of 35.5°. Five levels of 3-D ultrasonic anemometers were deployed at each tower and the eddy-covariance technique was utilized to directly measure turbulent momentum fluxes.

Well-developed katabatic flows were observed with jet-like wind profiles at all observational sites during clear sky and weak synoptic conditions, when the katabatic forcing due to radiative cooling dominates during the nighttime. Based on the location where slope-normal momentum fluxes approach zero, the jet peak heights were estimated assuming that the fluxes are co-gradient and hence change sign with the velocity profiles (Grachev et al., 2016). The median wind maxima heights were 6.15, 6.01, and 1.15 m for UT1, UT2, and Swiss sites, respectively. The estimations were also confirmed by inspecting stream-wise wind speed profiles.

Below the jet peak, where the vertical momentum flux was dominated by the surface stress generated from surface roughness, the magnitude of $\overline{u'w'}$ decreased significantly as the height increases at all three sites. We propose a modified flux-gradient relation for dimelsionless wind shear below the katabatic jet peak that incorporates slope angle. A tangent function of the slope angle was applied to the atmospheric stability parameters to account for differing slope angles at the two sites. The modified similarity function of dimensionless wind shear can be expressed as $\phi_m = 0.65\zeta_\alpha^{0.56} + 0.67$ below the jet peak. Given that the two sites have slope angles that differ by an order of magnitude and that the data collapse to an unprecedented degree for slope flows, this relation is an important improvement toward better katabatic flow simulations. RMSE of normalized momentum flux based on proposed relation and classic Businger et al. (1971) relation is 0.20 and 4.65, respectively.

The new findings will be particularly useful in prescribing the wall-model and/or turbulence closures in numerical simulations of katabatic flows (e.g., large-eddy simulations) and can be readily implemented. Like parameterizations for idealized terrain, advection may adversely impact the applicability of the proposed parameterization, and it may explain some of the scatter in Figure 4a. However, given that the data collapse quite well, advection likely has a negligible impact on the results. Hence the applicability, of the parameterization for very deep katabatic flows that form over much longer slopes (e.g., Antarctic slopes), for which advection maybe more significant, must be verified. Furthermore, given the sites used for the empirical analyses, we propose the modified similarity function for katabatic flows over mountain slopes with short vegetation. We speculate however, that it will also hold for mountain glaciers given that the glacier roughness may have a similar impact as the short and/or sparse vegetation (accounting for d_0 in Equation 5). This speculation will be tested in future studies. Further testing and experimentation are critical for katabatic flows below forest canopies. In addition, the parameterization is proposed for cases of katabatic flows when a clear jet-shaped velocity profile is evident and hence, is not intended for cases such as synoptically driven downslope winds or locations near mountain peaks.

Data Availability Statement

Open Research: The observational data are available through Hang and Oldroyd (2021).

References

Arya, P. S. (2001). *Introduction to micrometeorology*. Academic Press.
Aubinet, M., Vesala, T., & Papale, D. (2012). *Eddy covariance: A practical guide to measurement and data analysis*. Springer Netherlands.
Axelsen, S. L., & van Dop, H. (2009a). Large-eddy simulation of katabatic winds. Part 1: Comparison with observations. *Acta Geophysica*, *57*(4), 803–836. https://doi.org/10.2478/s11600-009-0041-6
Axelsen, S. L., & van Dop, H. (2009b). Large-eddy simulation of katabatic winds. Part 2: Sensitivity study and comparison with analytical models. *Acta Geophysica*, *57*(4), 837–856. https://doi.org/10.2478/s11600-009-0042-5
Babić, K., Klaić, Z. B., & Večenaj, Ž. (2012). Determining a turbulence averaging time scale by Fourier analysis for the nocturnal boundary layer. *Geofizika*, *29*, 35–51.
Bromwich, D. H., & Kurtz, D. D. (1984). Katabatic wind forcing of the terra nova bay polynya. *Journal of Geophysical Research*, *89*(4), 3561–3572. https://doi.org/10.1029/jc089ic03p03561
Businger, J. A., Wyngaard, J. C., Izumi, Y., & Bradley, E. F. (1971). Flux-profile relationships in the atmospheric surface layer. *Journal of the Atmospheric Sciences*, *28*(2), 181–189. https://doi.org/10.1175/1520-0469(1971)028<0181:fprita>2.0.co;2

Charrondière, C., Brun, C., Sicart, J. E., Cohard, J. M., Biron, R., & Blein, S. (2020). Buoyancy effects in the turbulence kinetic energy budget and reynolds stress budget for a katabatic jet over a steep Alpine slope. *Boundary-Layer Meteorology*, *177*(1), 97–122. https://doi.org/10.1007/s10546-020-00549-2

Chenge, Y., & Brutsaert, W. (2005). Flux profile relationships for wind speed and temperature in the stable atmospheric boundary layer. *Boundary-Layer Meteorology*, *114*(3), 519–538. https://doi.org/10.1007/s10546-004-1425-4

Clifton, A., Daniels, M. H., & Lehning, M. (2014). Effect of winds in a mountain pass on turbine performance. *Wind Energy*, *17*, 1543–1562. https://doi.org/10.1002/we.1650

Denby, B., & Smeets, C. J. P. P. (2000). Derivation of turbulent flux profiles and roughness lengths from katabatic flow dynamics. *Journal of Applied Meteorology*, *39*(9), 1601–1612. https://doi.org/10.1175/1520-0450(2000)039<1601:dotfpa>2.0.co;2

Dyer, A. J. (1974). A review of flux-profile relationships. *Boundary-Layer Meteorology*, *7*(3), 363–372. https://doi.org/10.1007/BF00240838

Ebner, L., Heinemann, G., Haid, V., & Timmermann, R. (2014). Katabatic winds and polynya dynamics at Coats Land, Antarctica. *Antarctic Science*, *26*(3), 309–326. https://doi.org/10.1017/S0954102013000679

Fernando, H. J. S., Pardyjak, E. R., Di Sabatino, S., Chow, F. K., De Wekker, S. F. J., Hoch, S. W., et al. (2015). The MATERHORN: Unraveling the intricacies of mountain weather. *Bulletin of the American Meteorological Society*, *96*(11), 1945–1967. https://doi.org/10.1175/bams-d-13-00131.1

Forrer, J., & Rotach, M. W. (1997). On the turbulence structure in the stable boundary layer over the Greenland ice sheet. *Boundary-Layer Meteorology*, *85*(1), 111–136. https://doi.org/10.1023/A:1000466827210

Giometto, M. G., Grandi, R., Fang, J., Monkewitz, P. A., & Parlange, M. B. (2017). Katabatic flow: A closed-form solution with spatially-varying eddy diffusivities. *Boundary-Layer Meteorology*, *162*(2), 307–317. https://doi.org/10.1007/s10546-016-0196-z

Grachev, A. A., Leo, L. S., Di Sabatino, S., Fernando, H. J. S., Pardyjak E. R., & Fairall C. W. (2016). Structure of turbulence in katabatic flows below and above the wind-speed maximum. *Boundary-Layer Meteorology*, *159*(3), 469–494. https://doi.org/10.1007/s10546-015-0034-8

Grisogono, B., & Axelsen, S. L. (2012). A note on the pure katabatic wind maximum over gentle slopes. *Boundary-Layer Meteorology*, *145*, 527–538. https://doi.org/10.1007/s10546-012-9746-1

Grisogono, B., Kraljevic, L., & Jericevi, A. (2007). Notes and correspondence the low-level katabatic jet height versus Monin–Obukhov height. *Quarterly Journal of the Royal Meteorological Society*, *133*, 2133–2136. https://doi.org/10.1002/qj.190

Grisogono, B., & Oerlemans, J. (2001a). Katabatic flow: Analytic solution for gradually varying eddy diffusivities. *Journal of the Atmospheric Sciences*, *58*(21), 3349–3354. https://doi.org/10.1175/1520-0469(2001)058<3349:kfasfg>2.0.co;2

Grisogono, B., & Oerlemans, J. (2001b). A theory for the estimation of surface fluxes in simple katabatic flows. *Quarterly Journal of the Royal Meteorological Society*, *127*(578), 2725–2739. https://doi.org/10.1002/qj.49712757811

Grisogono, B., & Rajak, D. Z. (2009). Assessment of Monin–Obukhov scaling over small slopes. *Geofizika*, *26*(1), 101–108.

Hang, C., Nadeau, D. F., Gultepe, I., Hoch, S. W., Román-Cascón, C., Pryor, K., & Pardyjak, E. R. (2016). A case study of the mechanisms modulating the evolution of valley fog. *Pure and Applied Geophysics*, *173*(9), 3011–3030. https://doi.org/10.1007/s00024-016-1370-4

Hang, C., Nadeau, D. F., Pardyjak, E. R., & Parlange, M. B. (2020). A comparison of near-surface potential temperature variance budgets for unstable atmospheric flows with contrasting vegetation cover flat surfaces and a gentle slope. *Environmental Fluid Mechanics*, *20*(5), 1251–1279. https://doi.org/10.1007/s10652-018-9647-z

Hang, C., & Oldroyd, H. J. (2021). *Katabatic flow data*. https://doi.org/10.7910/DVN/HIDISA

Heinemann, G. (2004). Local similarity properties of the continuously turbulent stable boundary layer over Greenland. *Boundary-Layer Meteorology*, *112*, 283–305. https://doi.org/10.1023/B:BOUN.0000027908.19080.b7

Högström, U. (1988). Non-dimensional wind and temperature profiles in the atmospheric surface layer: A re-evaluation. *Boundary-Layer Meteorology*, *42*, 55–78. https://doi.org/10.1007/bf00119875

Horst, T. W., & Doran, J. C. (1986). Nocturnal drainage flow on simple slopes. *Boundary-Layer Meteorology*, *34*(3), 263–286. https://doi.org/10.1007/BF00122382

Jensen, D. D., Nadeau, D. F., Hoch, S. W., & Pardyjak, E. R. (2017). The evolution and sensitivity of katabatic flow dynamics to external influences through the evening transition. *Quarterly Journal of the Royal Meteorological Society*, *143*(702), 423–438. https://doi.org/10.1002/qj.2932

Klipp, C. L., & Mahrt, L. (2004). Flux-gradient relationship, self-correlation and intermittency in the stable boundary layer. *Quarterly Journal of the Royal Meteorological Society*, *130*, 2087–2103. https://doi.org/10.1256/qj.03.161

Lee, S. M., Fernando, H. J. S., Princevac, M., Zajic, D., Sinesi, M., McCulley, J. L., & Anderson, J. (2003). Transport and diffusion of ozone in the nocturnal and morning planetary boundary layer of the Phoenix valley. *Environmental Fluid Mechanics*, *3*, 331–362. https://doi.org/10.1023/A:1023680216173

Lehner, M., Whiteman, C. D., Hoch, S. W., Crosman, E. T., Jeglum, M. E., Cherukuru, N. W., et al. (2016). The METCRAX II field experiment: A study of downslope windstorm-type flows in Arizona's Meteor Crater. *Bulletin of the American Meteorological Society*, *97*(2), pp.217–235. https://doi.org/10.1175/BAMS-D-14-00238.1

Łobocki, L. (2014). Surface-layer flux-gradient relationships over inclined terrain derived from a local equilibrium, turbulence closure model. *Boundary-Layer Meteorology*, *150*, 469–483. https://doi.org/10.1007/s10546-013-9888-9

Mahrt, L. (1998). Stratified atmospheric boundary layers and breakdown of models. *Theoretical and Computational Fluid Dynamics*, *11*, 263–279. https://doi.org/10.1007/s001620050093

Mahrt, L. (2014). Stably stratified atmospheric boundary layers. *Annual Review of Fluid Mechanics*, *46*(1), 23–45. http://www.annualreviews.org/doi/abs/10.1146/annurev-fluid-010313-141354

Monin, A. S., & Obukhov, A. M. (1954). Basic laws of turbulent mixing in the surface layer of the atmosphere. *Contributions of the Geophysical Institute of the Academy of Sciences of the USSR*, *24*(151), 163–187.

Monti, P., Fernando, H. J. S., Princevac, M., Chan, W. C., Kowalewski, T. A., & Pardyjak, E. R. (2002). Observations of flow and turbulence in the nocturnal boundary layer over a slope. *Journal of the Atmospheric Sciences*, *59*(17), 2513–2534. https://doi.org/10.1175/1520-0469(2002)059<2513:oofati>2.0.co;2

Nadeau, D. F., Pardyjak, E. R., Higgins, C. W., & Parlange, M. B. (2013). Similarity scaling over a steep alpine slope. *Boundary-Layer Meteorology*, *147*(3), 401–419. https://doi.org/10.1007/s10546-012-9787-5

Nieuwstadt, F. T. M. (1984). The turbulent structure of the stable, nocturnal boundary layer. *Journal of the Atmospheric Sciences*, *41*, 2202–2216. https://doi.org/10.1175/1520-0469(1984)041<2202:ttsots>2.0.co;2

Obukhov, A. M. (1971). Turbulence in an atmosphere with a non-uniform temperature. *Boundary-Layer Meteorology*, *2*, 7–29. https://doi.org/10.1007/BF00718085

Oerlemans, J., Björnsson, H., Kuhn, M., Obleitner, F., Palsson, F., Smeets, C. J. P. P., et al. (1999). Glacio-meteorological investigations on Vatnajökull, Iceland, summer 1996: An overview. *Boundary-Layer Meteorology*, *92*(1), 3–24. https://doi.org/10.1023/a:1001856114941

Oldroyd, H. J., Katul, G., Pardyjak, E. R., & Parlange, M. B. (2014). Momentum balance of katabatic flow on steep slopes covered with short vegetation. *Geophysical Research Letters*, *41*(13), 4761–4768. https://doi.org/10.1002/2014GL060313

Oldroyd, H. J., Pardyjak, E. R., Higgins, C. W., & Parlange, M. B. (2016). Buoyant turbulent kinetic energy production in steep-slope katabatic flow. *Boundary-Layer Meteorology*, *161*(3), 405–416. https://doi.org/10.1007/s10546-016-0184-3

Oldroyd, H. J., Pardyjak, E. R., Huwald, H., & Parlange, M. B. (2016). Adapting tilt corrections and the governing flow equations for steep, fully three-dimensional, mountainous terrain. *Boundary-Layer Meteorology*, *159*(3), 539–565. https://doi.org/10.1007/s10546-015-0066-0

Papadopoulos, K. H., Helmis, C. G., Soilemes, A. T., Kalogiros, J., Papageorgas, P. G., & Asimakopoulos, D. N. (1997). The structure of katabatic flows down a simple slope. *Quarterly Journal of the Royal Meteorological Society*, *123*(542), 1581–1601. https://doi.org/10.1002/qj.49712354207

Pardyjak, E. R., Fernando, H. J. S., Hunt, J. C. R., Grachev, A. A., & Anderson, J. (2009). A case study of the development of nocturnal slope flows in a wide-open valley and associated air quality implications. *Meteorologische Zeitschrift*, *18*(1), 85–100. https://doi.org/10.1127/0941-2948/2009/362

Paterson, J. T., Rotella, J. J., Arrigo, K. R., & Garrott, R. A. (2015). Tight coupling of primary production and marine mammal reproduction in the Southern Ocean. *Proceedings of the Royal Society B: Biological Sciences*, *282*. https://doi.org/10.1098/rspb.2014.3137

Prandtl, L. (1942). *Führer durch die Strömungslehre*. Vieweg and Sohn.

Pypker, T. G., Unsworth, M. H., Mix, A. C., Rugh, W., Ocheltree, T., Alstad, K., & Bond, B. J. (2007). Using nocturnal cold air drainage flow to monitor ecosystem processes in complex terrain. *Ecological Applications*, *17*(3), 702–714. https://doi.org/10.1890/05-1906

Román-Cascón, C., Yagüe, C., Mahrt, L., Sastre, M., Steeneveld, G. J., Pardyjak, E., & Hartogensis, O. (2015). Interactions among drainage flows, gravity waves and turbulence: A BLLAST case study. *Atmospheric Chemistry and Physics*, *15*(15), 9031–9047. https://doi.org/10.5194/acp-15-9031-2015

Shapiro, A., & Fedorovich, E. (2014). A boundary-layer scaling for turbulent katabatic flow. *Boundary-Layer Meteorology*, *153*(1), 1–17. https://doi.org/10.1007/s10546-014-9933-3

Smeets, C. J. P. P., Duynkerke, P. G., & Vugts, H. F. (1998). Turbulence characteristics of the stable boundary layer over a mid-latitude glacier. Part I: A combination of katabatic and large-scale forcing. *Boundary-Layer Meteorology*, *87*(1), 117–145. https://doi.org/10.1023/A:1000860406093

Stiperski, I., Holtslag, A. A. M., Lehner, M., Hoch, S. W., & Whiteman, C. D. (2019). On the turbulence structure of deep katabatic flows on a gentle mesoscale slope. *Quarterly Journal of the Royal Meteorological Society*, *146*, 1–26. https://doi.org/10.1002/qj.3734

Stull, R. B. (1988). *An introduction to boundary layer meteorology*. Springer Netherlands.

van den Broeke, M. R. (1997). Momentum, heat, and moisture budgets of the katabatic wind layer over a midlatitude glacier in summer. *Journal of Applied Meteorology*, *36*(6), 763–774. https://doi.org/10.1175/1520-0450(1997)036<0763:mhambo>2.0.co;2

van der Avoird, E., & Duynkerke, P. G. (1999). Turbulence in a katabatic flow. *Boundary-Layer Meteorology*, *92*(1), 39–66. https://doi.org/10.1023/a:1001744822857

Vickers, D., & Mahrt, L. (2003). The cospectral gap and turbulent flux calculations. *Journal of Atmospheric and Oceanic Technology*, *20*, 660–672. https://doi.org/10.1175/1520-0426(2003)20<660:tcgatf>2.0.co;2

Wenta, M., & Cassano, J. J. (2020). The atmospheric boundary layer and surface conditions during katabatic wind events over the Terra Nova Bay Polynya. *Remote Sensing*, *12*(24), 4160. https://doi.org/10.3390/rs12244160

Whiteman, C. D. (2000). *Mountain meteorology: Fundamentals and applications*. Oxford University Press.

Wilczak, J., Oncley, S., & Stage, S. (2001). Sonic anemometer tilt correction algorithms. *Boundary-Layer Meteorology*, *99*(1), 127–150. https://doi.org/10.1023/a:1018966204465